LCC – 0055 02/01
CBP Tech Note-223

Linear Collider Collaboration Tech Notes

Improved Dynamics in the 180 Hz NLC Damping Rings

February 2001

Andrzej Wolski
Lawrence Berkeley National Laboratory
Berkeley, California

Abstract: Adding a field gradient to the main dipoles for the NLC Main Damping Ring lattice has leads to significant improvements in the dynamic behavior of particles in the lattice. We describe the properties of the new lattice, including some initial estimates of alignment tolerances required to achieve the desired vertical emittance.

CBP Tech Note-223
LCC-0055

Improved Dynamics in the 180 Hz NLC Damping Rings

Andrzej Wolski
Lawrence Berkeley National Laboratory

February 5th, 2000

Abstract

Adding a field gradient to the main dipoles for the NLC Main Damping Ring lattice has led to significant improvements in the dynamic behavior of particles in the lattice. We describe the properties of the new lattice, including some initial estimates of alignment tolerances required to achieve the desired vertical emittance.

1 Introduction

A previous note[1] described a lattice for the NLC Main Damping Rings, which would achieve the required damping at 180 Hz repetition rate. The length of the damping wiggler was kept to a realistic value by operating a pair of damping rings in each of the two injector systems (for electron and positrons). Each ring would operate at 90 Hz, storing two bunch trains, giving a combined 180 Hz rep rate; the design did not preclude operating the rings either in series or in parallel. While the design met the criteria in terms of damping rate, the dynamic aperture was a remaining concern. To achieve good injection efficiency, the target for the dynamic aperture is fifteen times the injected beam size horizontally and vertically. Although this was (just) achieved horizontally, a factor four improvement was required vertically.

Earlier studies[2] for the 120 Hz damping rings had shown significant benefits from allowing the arcs to be constructed from cells based on combined function dipoles, rather than bending magnets without gradient as in the initial 90 Hz design. This formed the basis for the improved design. The significant changes are then as follows:

- focusing gradient included in the main dipoles, to improve dynamics;
- basic TME cell modified from a four-quadrupole to a three-quadrupole design, to save space and cost;
- inclusion of a circumference-correction chicane in the injection/extraction straight;
- re-tuning of the straights to reduce the beta functions (and hence the chromaticity) and to achieve a more favorable phase advance;
- overall circumference reduced, to give some benefit in damping rate.

This note describes the structure and properties of the present lattice, and presents the results of some initial estimates of the alignment tolerances required to achieve the desired vertical emittance. For the present studies, we continued to model the wiggler as a sequence of linear elements; investigations leading to a more sophisticated model are in progress.

2 Lattice Parameters

The "external" parameters driving the lattice design are shown in Table 1. The principal lattice parameters are shown in Table 2.

Table 1: "External" parameters.

Bunches per train	N_b	95
bunch-to-bunch spacing[a]	τ_b /ns	2.8
kicker rise/fall time	τ_k /ns	65
collider repetition rate	f /Hz	180
injected horizontal/vertical emittance	$\gamma\varepsilon_{inj}$ /mm mrad	150
extracted horizontal emittance	$\gamma\varepsilon_{x,ext}$ /mm mrad	<3
extracted vertical emittance[b]	$\gamma\varepsilon_{y,ext}$ /mm mrad	<0.03

[a] At this bunch spacing, every alternate RF bucket is filled. A high luminosity upgrade to the NLC will fill every bucket, giving a bunch spacing of 1.4 ns.

[b] An increased luminosity may be achieved by reducing the extracted vertical emittance to 0.02 mm mrad.

Table 2: Principal lattice parameters.

Energy	E /GeV	1.98
Number of bunch trains stored	N_{train}	2
Store time	N_τ	4.76
Circumference	C /m	199.863
Arc cell type		TME
Arc cell length	/m	3.737
Length of each straight	/m	33.163
Number of arc cells		34 + 4×½
Dipole gradient	k_1 /m^2	-1.0
Horizontal tune	Q_x	25.1242
Vertical tune	Q_y	9.7210
Natural horizontal chromaticity	ξ_x	-31.22
Natural vertical chromaticity	ξ_y	-35.10
Normalized natural emittance	$\gamma\varepsilon_0$ /mm mrad	2.62
Damping times	τ_x, τ_y /ms	4.36, 4.67
Assumed coupling	κ	0.65 %
Extracted horizontal emittance	$\gamma\varepsilon_{x,ext}$ /mm mrad	2.62
Extracted vertical emittance	$\gamma\varepsilon_{y,ext}$ /mm mrad	0.0280
Ratio of vertical equilibrium to extracted emittance	$\varepsilon_{y0}/\varepsilon_{y,ext}$	0.61
Momentum compaction	α	4.62×10^{-4}

RF voltage	V_{rf} /MV	0.844
RF acceptance	ε_{rf}	1.5 %
Rms energy spread	σ_δ	0.0885 %
Bunch length	σ_z /mm	3.91
Wiggler peak field	$\hat{B}_w$ /T	2.15
Wiggler period	λ_w /m	0.27
Wiggler total length	L_w /m	27.744
Integrated wiggler field	$\int \hat{B}_w^2 ds$ /T^{2}m	64.12
Energy loss/turn from dipoles	U_0/keV	247
Energy loss/turn from wiggler	U_w/keV	318
Total energy loss/turn	$U_0 + U_w$ /keV	565
Energy loss ratio	F_w	1.29
Dynamic aperture	A	$15\sigma_{inj}$

Lattice functions for different sections of the lattice are shown in Figure 1 through Figure 4 below.

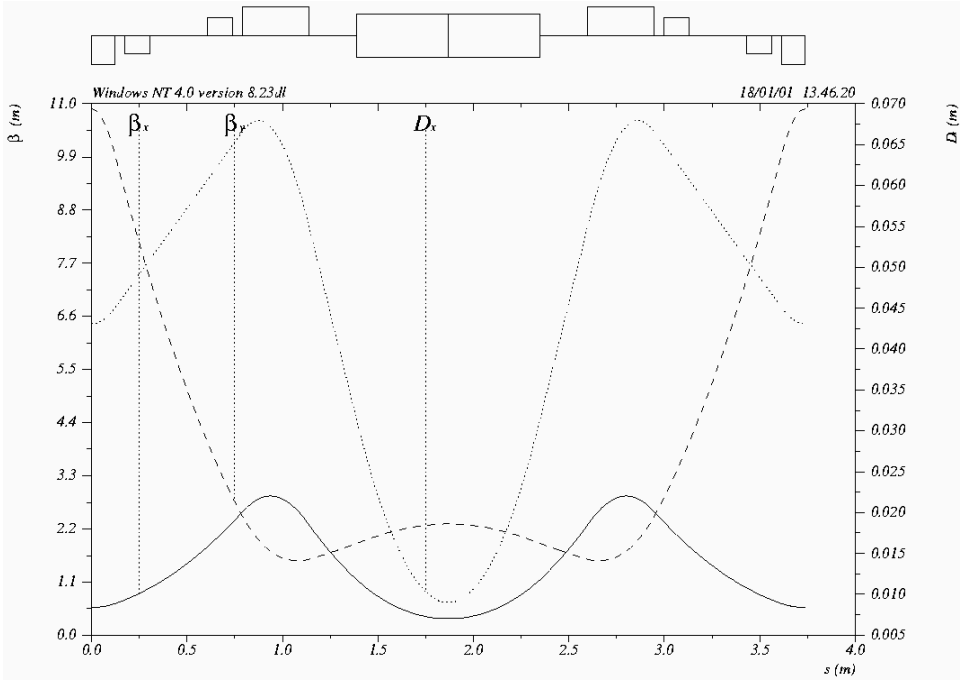

Figure 1

Lattice functions in an arc (TME) cell.

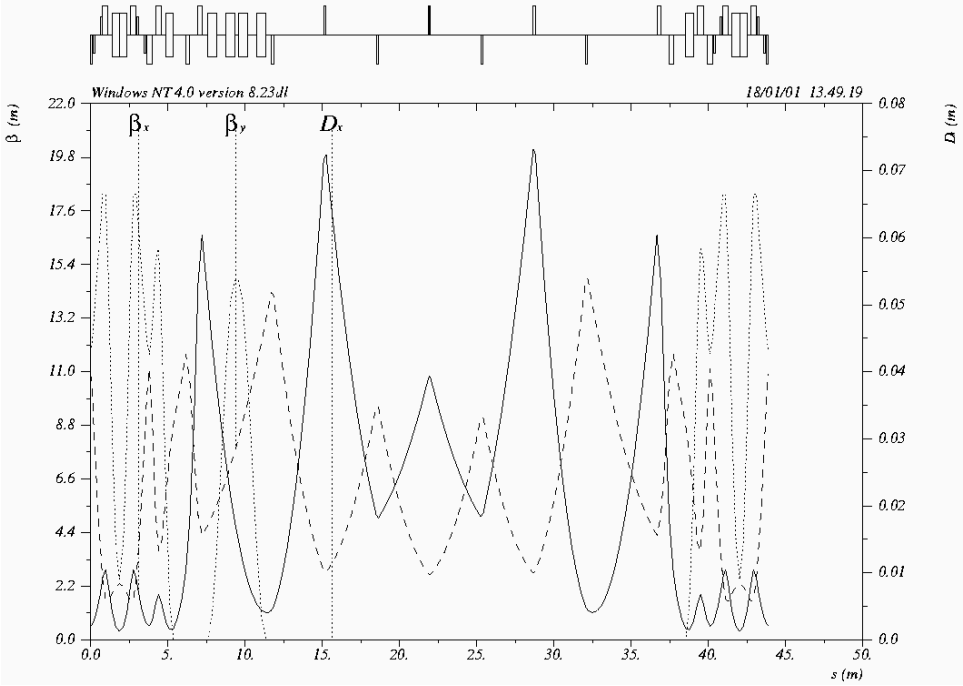

Figure 2

Lattice functions in the injection/extraction straight. A full TME cell is shown on either end of the straight. The circumference correction chicane appears as a sequence of four dipoles towards the left side of the diagram.

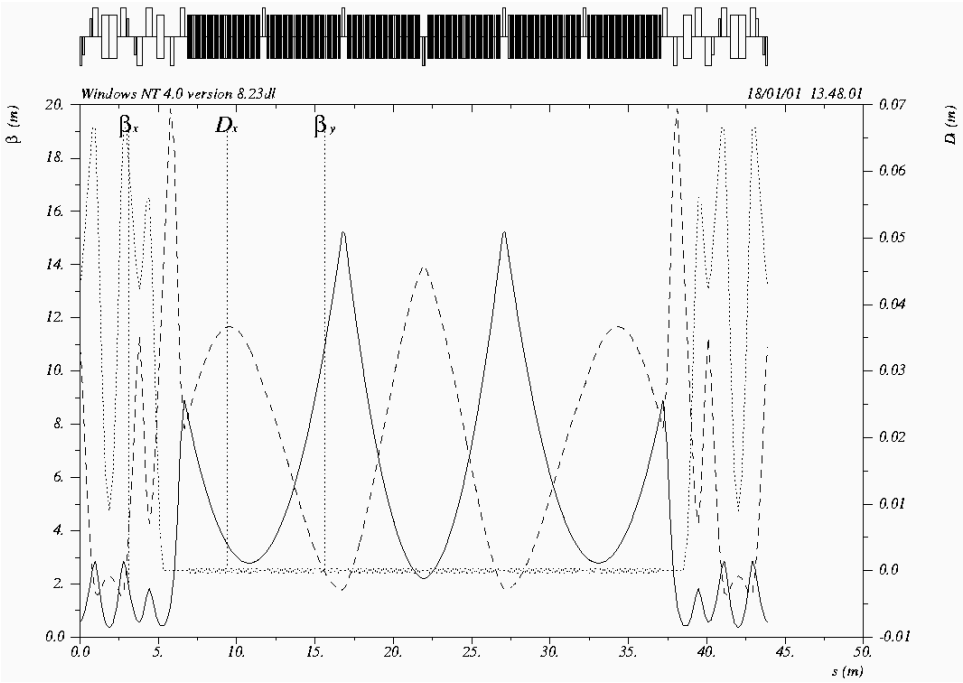

Figure 3

Lattice functions through the wiggler straight. A full TME cell is shown on either end.

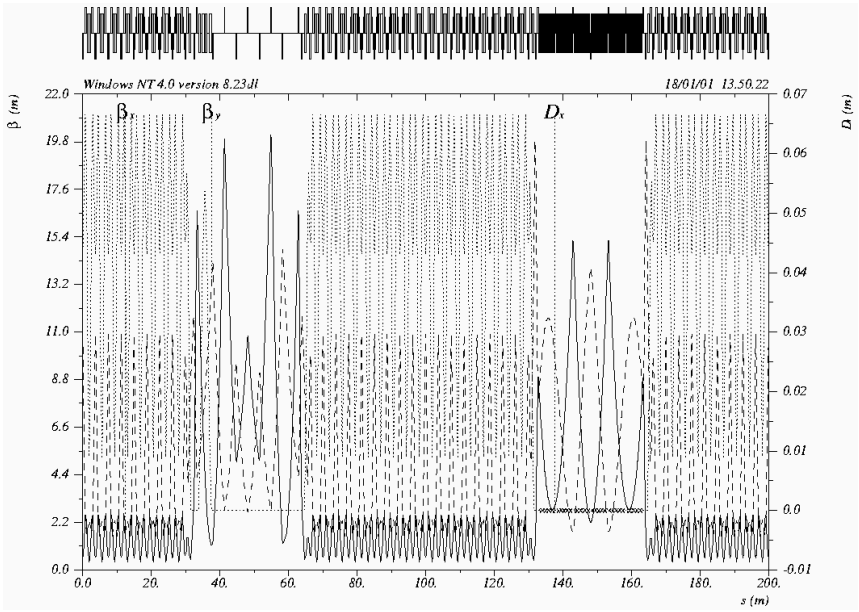

Figure 4

Lattice functions for the complete lattice.

3 Chromatic Properties

Although the sextupoles are adjusted to give zero first-order chromaticity, the tune shift with momentum can still be significant, as a result of large higher order chromaticity. The variation of horizontal and vertical tune with momentum deviations up to ±1.5% are shown in Figure 5, and the working point in tune space is shown in Figure 6.

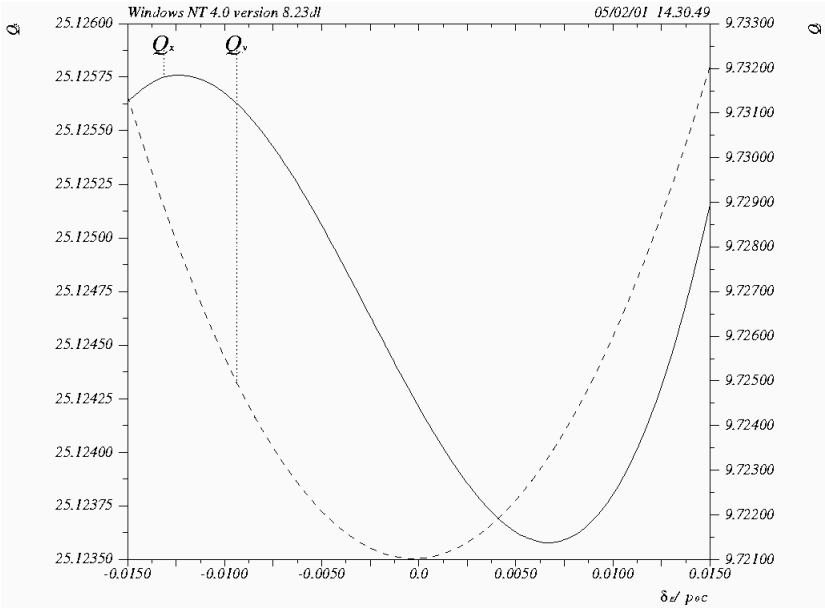

Figure 5

Variation of tunes with momentum, up to ±1.5% momentum deviation.

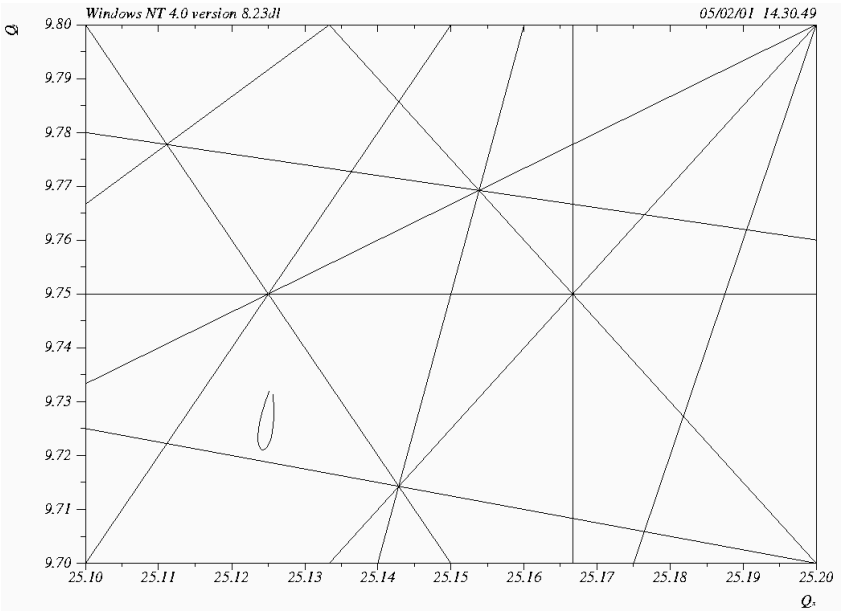

Figure 6

Working point of the lattice in tune space. The curved line shows variation of the tune with momentum deviations up to ±1.5%. Resonance lines up to sixth order are shown.

We note that the lattice tunes have a strong effect on the magnet alignment tolerances, and integer and half-integer values in particular are to be avoided. In this respect, the present working point appears reasonable.

4 Dynamic Aperture

The damping ring must have a good dynamic aperture to minimize particle loss, particularly during injection. The aperture is limited by the sextupoles, which are used in the dispersive regions (the arcs) to correct chromaticity, and tuned to give the lattice zero chromaticity. If the straight sections are assumed to contain only linear elements, and are tuned to give exact integer phase advances horizontally and vertically, then the dynamics of the lattice reduces to the dynamics of the TME cell. This has been achieved in the current lattice design, with the phase advances over both the injection/extraction straight and the wiggler straight very close to 2.0 horizontally, and 1.0 vertically. The chromaticities of the straights are relatively low (-2.9 (–1.8) horizontally (vertically) for the injection/extraction straight, and –1.9 (-2.6) for the wiggler straight), so the variation from the integer condition is small for momentum deviations up to 1.5%.

Horizontal phase space portraits are shown in Figure 7, and vertical phase space portraits in Figure 8, for a single arc cell and for the full lattice. The portraits for a single cell are remarkably similar to those for the full lattice, indicating the success of the tuning of the straight sections to integer values, in the approximation where all elements in the straights are linear.

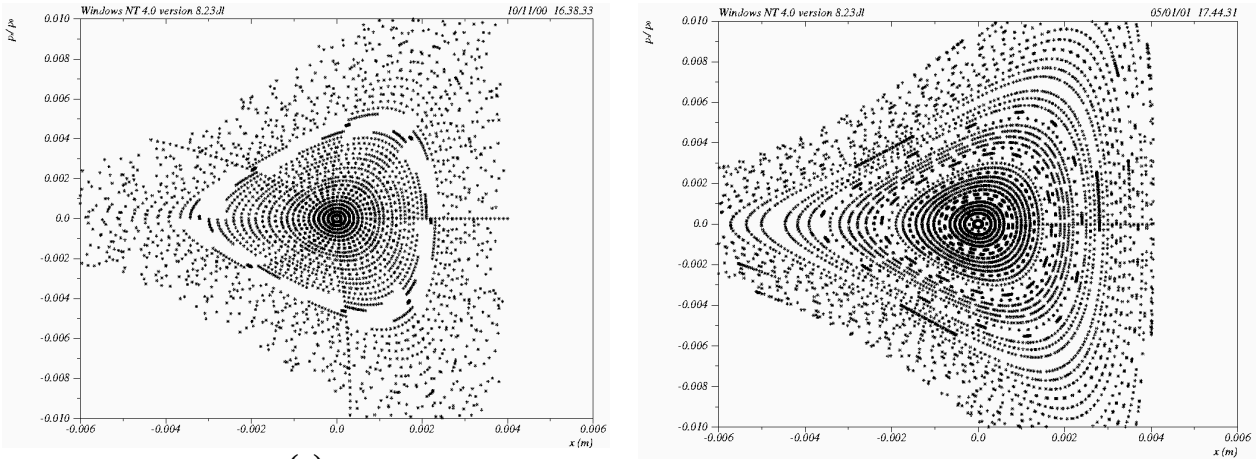

(a) (b)

Figure 7

Horizontal phase space portraits for (a) a single arc cell and (b) the full lattice. The observation point is the center of the DQUAD in an arc cell (as shown in Figure 1, where β_x = 0.574 m.

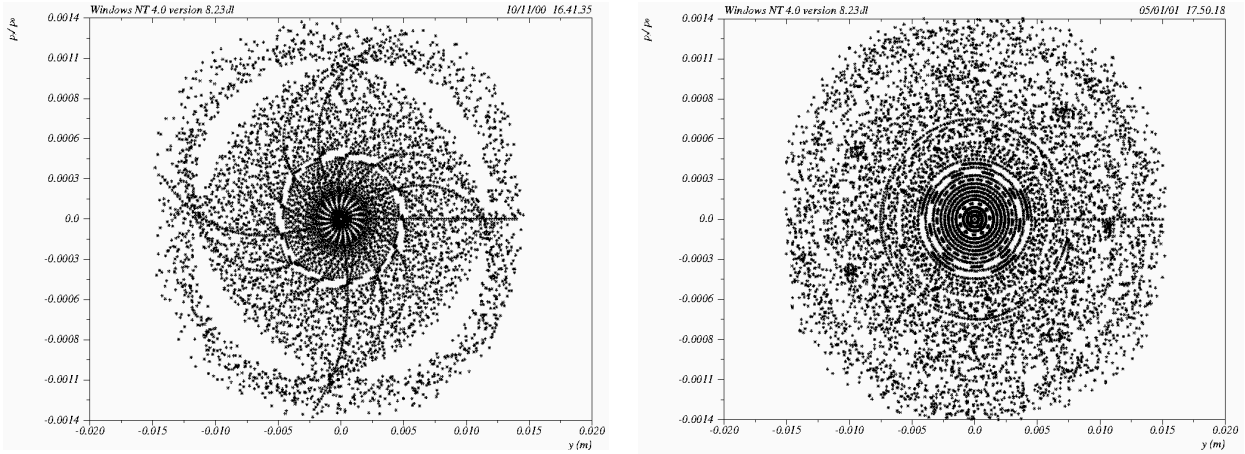

(a) (b)

Figure 8

Vertical phase space portraits for (a) a single arc cell and (b) the full lattice. The observation point is the center of the DQUAD in an arc cell (as shown in Figure 1), where β_y = 10.901 m.

Optimization of the dynamic aperture has been carried out pragmatically on a single TME cell, by adjusting the working point, and the phase advance between the sextupoles, to identify a region that gives good horizontal and vertical stability. However, a rigorous scan of tune space has not been carried out. As had been hoped, the inclusion of a horizontally defocusing gradient in the dipole significantly improves the stability of the dynamics. The reasons for this have not been decided conclusively, although some benefit is certainly derived from the reduction in the beta functions, leading to lower chromaticity, and hence lower sextupole strengths. We do not feel, though, that this fully explains the situation, since the integrated sextupole strengths have been reduced by approximately 20% over the previous lattice design, while the vertical dynamic aperture has increased more than a factor of four.

A dynamic aperture plot for the full lattice is shown in Figure 9. Again, we emphasize that the plot has been produced by tracking the wiggler as a linear element.

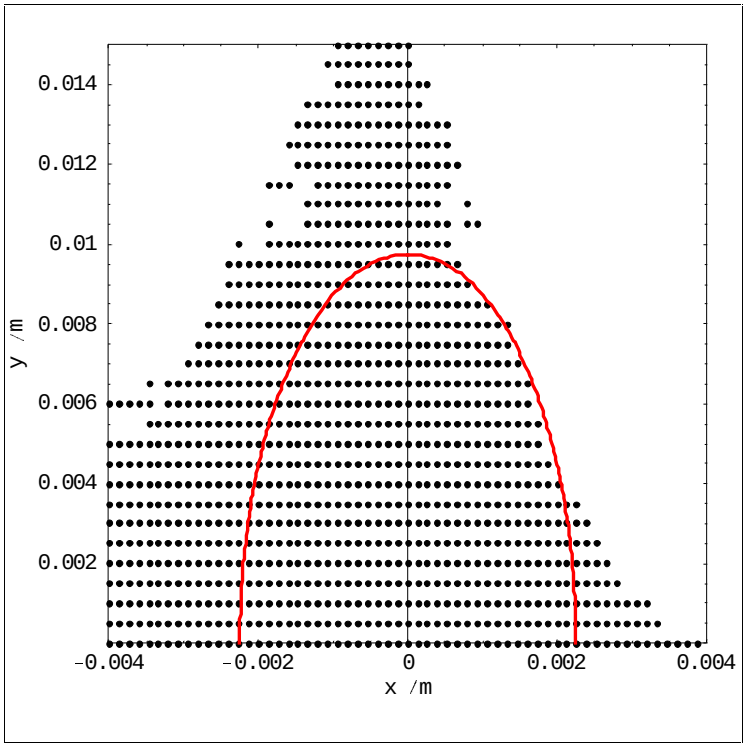

Figure 9

Dynamic aperture of the full lattice, with the wiggler modeled as a linear element. The particles were tracked through 200 turns, with the observation point at the center of the DQUAD in an arc cell, where β_x = 0.574 m and β_y = 10.901 m. The half ellipse shows 15 times the injected beam size.

The dynamic aperture is limited by the nonlinearities in the arc cells, and (particularly for the vertical motion) the matching across the straight sections. Assuming that the straight sections can be modified to give more favorable phase advances, we must look at the arc cells if we are to improve the dynamic aperture significantly. At present, we limit ourselves to characterizing the arc cells in terms of the tune dependence on amplitude.

The tune shifts with amplitude in the horizontal and vertical planes are shown in Figure 10 and Figure 11 respectively. A quartic fit is made to the data points for the horizontal dynamics, and a quadratic fit is made for the vertical dynamics. In both cases, the tune shifts with amplitude have been significantly reduced, compared to the case of no gradient in the dipole (the coefficients of quadratic terms were –1021 and 2656 horizontally and vertically – note that the vertical tune shift has therefore been reduced by nearly two orders of magnitude).

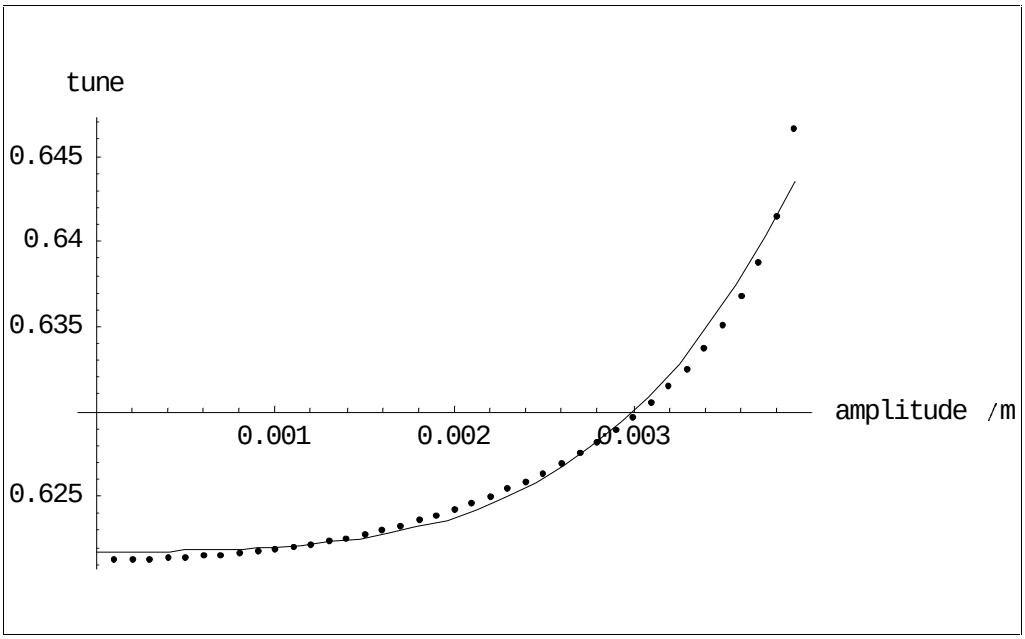

Figure 10

Horizontal tune shift with amplitude. The data points are fitted with a quadratic curve, of the form $0.62173+336x^2+1.66\times10^8x^4$.

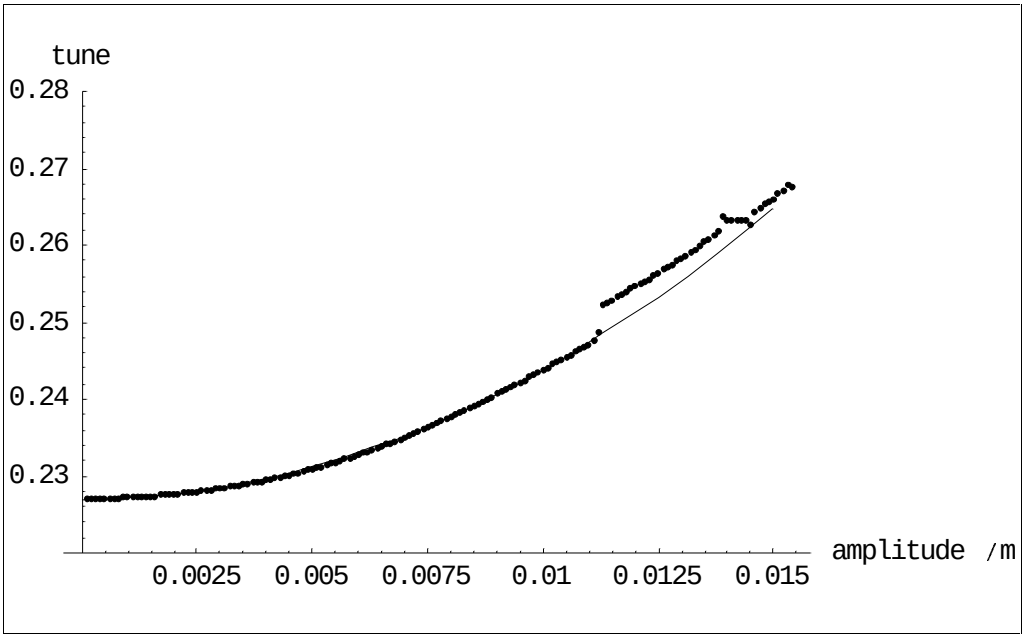

Figure 11

Vertical tune shift with amplitude. The data points are fitted with a quadratic curve, of the form $0.22691+336y^2$.

More information on the dynamics can be revealed by a frequency map analysis; this is shown in Figure 12. The plot is produced by setting up a regular grid of 4000 particles in co-ordinate space, from –2 mm to +2 mm horizontally, and from 0 mm to 3 mm

vertically. The particles are tracked for 256 passes through an arc cell, and the tunes determined by Fourier analysis. Resonance lines up to eighth order are shown on the plot; the driving resonances show up clearly, particularly the fourth order vertical resonance.

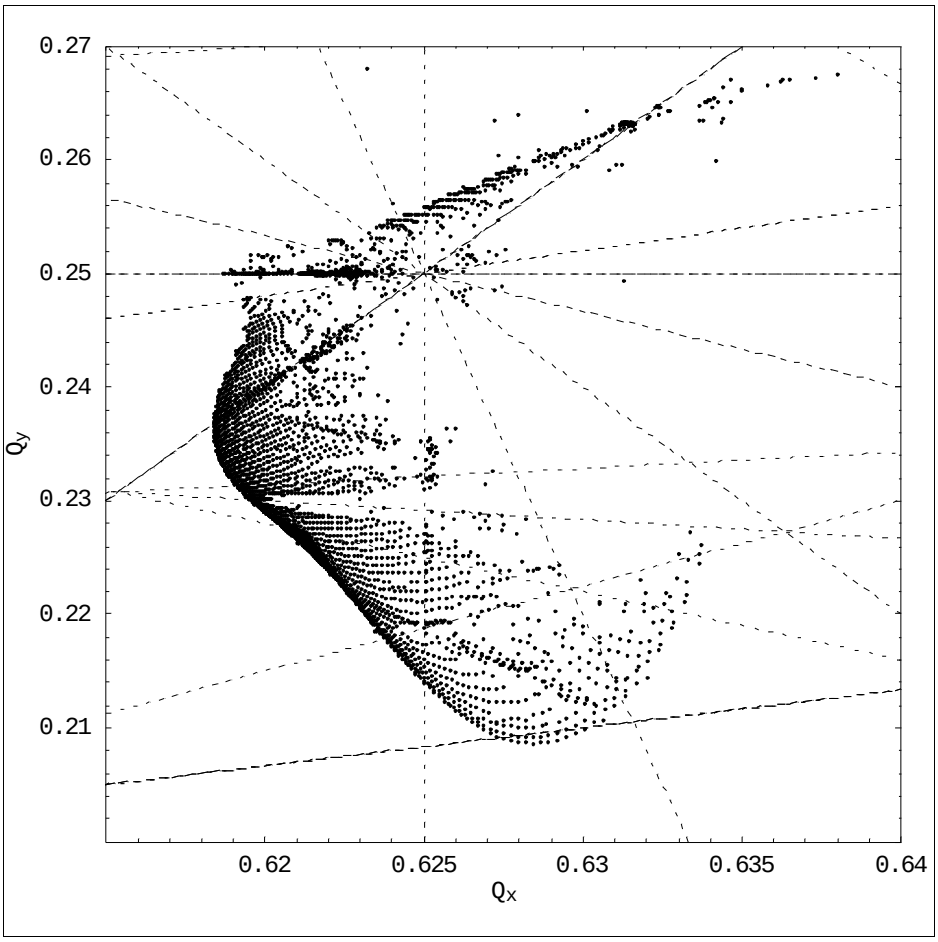

Figure 12

Frequency map analysis of an arc cell. Resonance lines up to eighth order are shown.

5 Circumference Correction Chicane

A chicane provides the possibility of making small corrections to the circumference without needing to adjust the RF frequency. The relatively small momentum compaction intrinsic in rings with low emittance, makes the damping rings very sensitive to changes in circumference arising from, for example, thermal effects. The energy is related to the circumference through:

$$\frac{\Delta E}{E_0} = -\frac{1}{\alpha}\frac{\Delta C}{C_0}$$

where α is the momentum compaction, which has the value 4.62×10^{-4}. Thus, a change in circumference of 1 mm leads to an energy change of 1% in the beam energy, which could have a significant impact on the beam dynamics. The ATF has observed variations

in circumference of ±3 mm over the course of several months. A particular design of chicane, consisting of a sequence of four bending magnets, has been considered by Emma and Raubenheimer[3], who showed that the effects of such a chicane on other damping ring parameters (such as emittance, bunch length and energy spread) are generally small. A recent design for the 120 Hz damping rings included a chicane that allowed correction of the circumference over a range[4,5] ±2 mm. This allowed the circumference of the ring to be restored in the event the wiggler is switched off ($\Delta C \approx -1.7\,\mathrm{mm}$). In our current design for 180 Hz, the shorter wiggler produces a circumference change of –1.3 mm, given by:

$$\Delta C \approx -\frac{1}{4}\frac{L_w}{\rho_w^2 \kappa_w^2}$$

where L_w is the wiggler total length, ρ_w the wiggler peak field bending radius, and κ_w the wiggler wave number. We have therefore taken the conservative approach of adopting the chicane design without modification; the length of the chicane in the 120 Hz design is 3.6 m, and this fits well into one section of the injection/extraction straight, allowing space of 0.34 m on either side to the nearest quadrupoles. In our design work, we set the chicane dipoles to nominal values, and calculated all parameters accordingly. The values presented in this note all include the effects of the circumference chicane. Adjustment of the chicane length necessitates a small retuning of the nearest quadrupole on the side nearest the arc, to compensate the focusing effects.

6 Initial Estimates of Alignment Tolerances

Achieving low vertical extracted emittance is a crucial performance target of the main damping rings. Low natural emittance and a sufficiently long store time are of course pre-requisites for achieving this target, but the emittance achieved will ultimately depend on the coupling between the horizontal and vertical planes. An assumed coupling of 0.65% in the present lattice will give the required extracted emittance of below 0.03 mm mrad, and it is important to understand whether this will be achievable in practice.

For our present studies, we have considered only coupling arising from the beam passing through the sextupoles with some vertical offset. This is expected to be the major source of coupling, though other sources, including quadrupole rotations around the beam axis, will have to be included in a more rigorous study. The vertical offset of the beam through the sextupoles may arise either from vertical alignment errors of the sextupoles themselves, or vertical alignment errors of the quadrupoles, giving vertical steering and hence closed orbit distortion. Note that vertical closed orbit distortion also contributes directly to vertical emittance through the generation of vertical dispersion (and the horizontal dispersion can also be coupled into the vertical plane by sextupole alignment errors and quadrupole rotations). For the present, though, we assume that the dominant contribution to the vertical emittance comes from orbit coupling; our results below provide some justification for this assumption.

To carry out the investigations, we extended the C++ class library MERLIN[6], to include Chao's method[7] of calculating the equilibrium emittances. MERLIN has been developed to provide powerful tools for constructing lattice models, including effects such as

magnet misalignments, and studying the dynamics of particles within those models. It does not, at present, give the lattice functions, although the closed orbit, and the single-turn transfer map linearised about the closed orbit can be found readily. Chao's method, depending on the eigenvectors of the transfer matrix, seemed therefore the most appropriate way of extending the library to allow calculation of the equilibrium emittances. In particular, it provides complete information on the equilibrium beam distribution in an arbitrarily misaligned and coupled lattice, including effects such as betatron and dispersion coupling without requiring knowledge of the lattice functions.

To begin with, we looked at the rms closed orbit deviation arising from quadrupole misalignments; this included the effects of sextupoles, though the sextupoles themselves were not misaligned. As we shall see, the closed orbit deviations we are interested in from point of view of coupling, range up to the order of 50 μm; this corresponds to quadrupole misalignments of a few microns, as seen from Figure 13 and Figure 14.

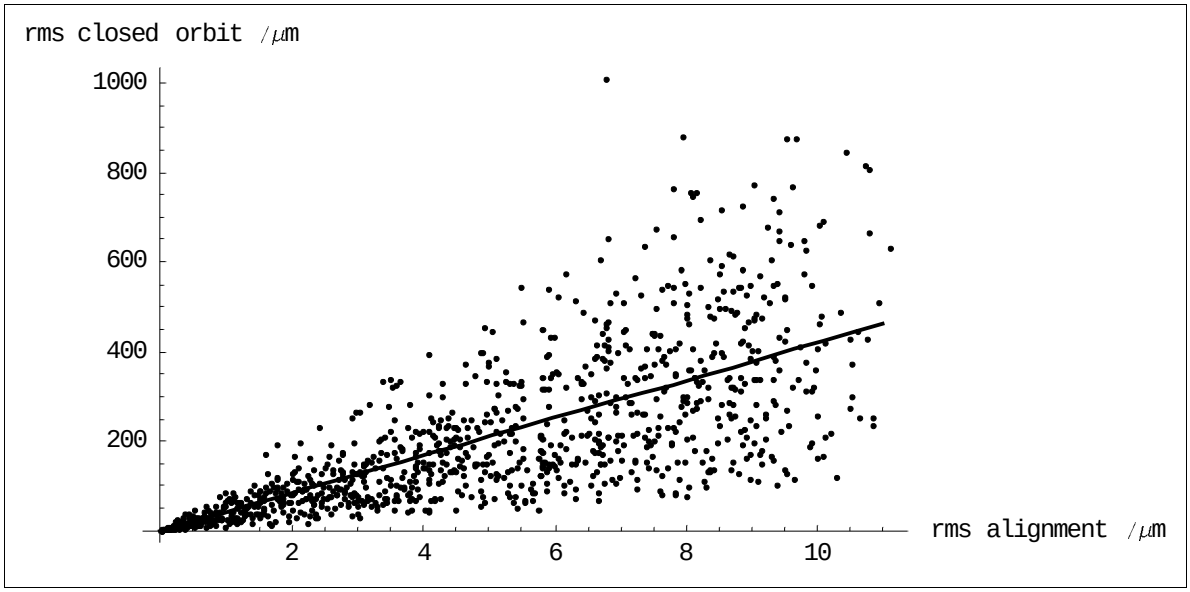

Figure 13

RMS horizontal closed orbit deviations arising from horizontal quadrupole misalignments, 1000 seeds. The line shows a fit of the form $y = 42.05\,x$

The horizontal rms closed orbit is roughly 40 times the rms quadrupole misalignment, while the vertical rms closed orbit is roughly 30 times the rms quadrupole misalignment. These values are consistent with the results of similar studies for the 120 Hz damping rings[8]. To study the effects of misalignments on the equilibrium vertical emittance, we applied horizontal and vertical misalignments to the quadrupoles of between 1 and 2 microns rms, and plotted the resulting equilibrium vertical emittance against the rms vertical closed orbit deviation. The results are shown in Figure 15. A quadratic fit to the data matches the correlation very well, and is in agreement with a simple semi-analytical model we can construct as follows.

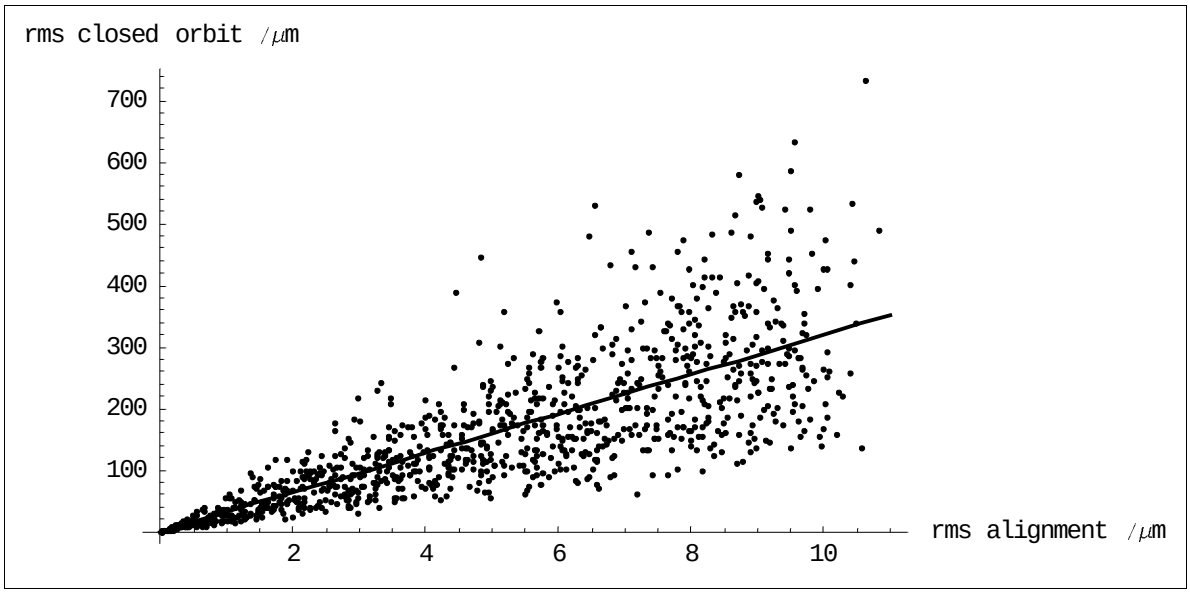

Figure 14

RMS vertical closed orbit deviations arising from vertical quadrupole misalignments, 1000 seeds. The line shows a fit of the form $y = 31.98\,x$

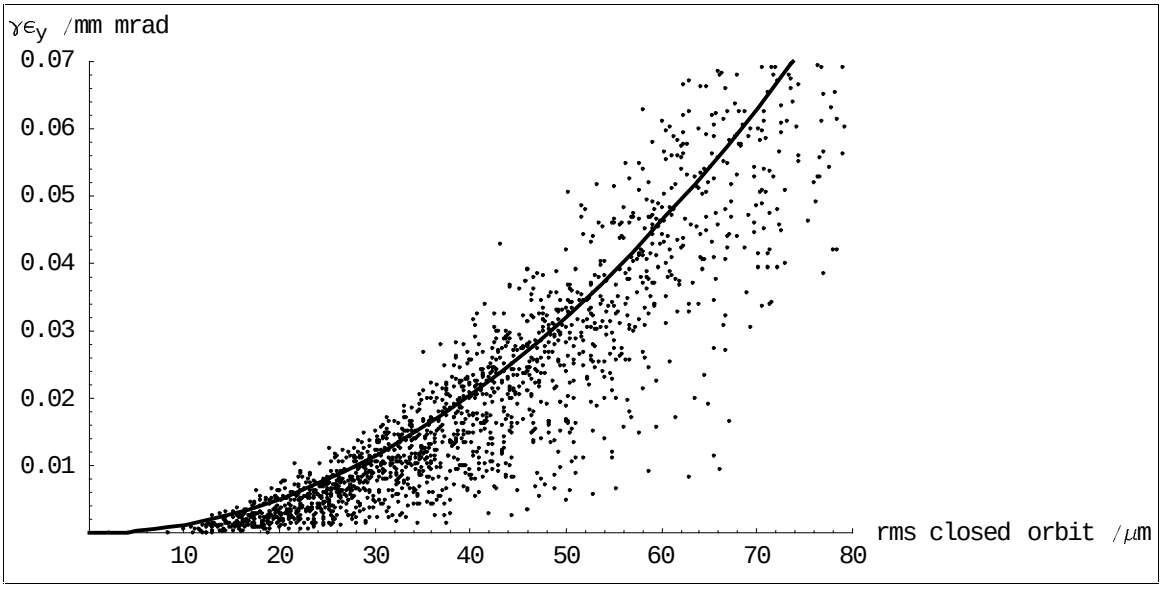

Figure 15

Equilibrium vertical emittance as a function of vertical rms closed orbit, 2000 seeds. The curve shows a best fit of the form $\gamma\varepsilon_y = 12.9\overline{y^2}$

Let us consider a cell containing a single sextupole, which is vertically displaced a distance δy. The generator for a single-pass map through the cell, starting at the sextupole location, may be written up to second order (after normalization):

$$H = \tfrac{1}{2}\mu_x\left(x^2 + p_x{}^2\right) + \tfrac{1}{2}\mu_y\left(y^2 + p_y{}^2\right) + k_2 l\sqrt{\beta_x\beta_y}\,xy\cdot\delta y$$

where the phase advance across the cell horizontally(vertically) is $\mu_x(\mu_y)$, and we have neglected chromatic effects We note that coupling of dispersion into the vertical plane is often a significant source of vertical emittance. However, the chromatic and betatron coupling terms appear very similar, and to obtain an order of magnitude estimate, we shall, for simplicity, consider only the betatron coupling. Given a map of the form

$$H = \tfrac{1}{2}\mu_x\left(x^2 + {p_x}^2\right) + \tfrac{1}{2}\mu_y\left(y^2 + {p_y}^2\right) + \kappa xy$$

a simple treatment of the betatron coupling, considering only the lowest order difference resonance, gives

$$g = \frac{\kappa^2}{\frac{1}{2}\Delta^2 + \kappa^2}$$

where $g = \varepsilon_y / \varepsilon_x$ is the coupling, and

$$\Delta = \left|\mu_x - \mu_y\right|$$

Thus, assuming $g << 1$, we can write:

$$g = 2\left(\frac{k_2 l}{\Delta}\right)^2 \beta_x \beta_y \cdot \delta y^2$$

If the cell contains N sextupoles, and the lattice is constructed simply by repeating the cell, then we can assume an effective coupling term in the generator:

$$\begin{aligned}\kappa xy &= N\sqrt{\overline{\left(k_2 l\sqrt{\beta_x\beta_y}\,\delta y\right)^2}}\,xy \\ &\approx N\sqrt{\overline{\left(k_2 l\sqrt{\beta_x\beta_y}\right)^2}}\,\sqrt{\overline{\delta y^2}}\,xy\end{aligned}$$

where we have made a rather gross approximation in factoring out the rms displacement. The nature of this approximation leads us to expect that we shall overestimate the coupling from this model; however, this may compensate for some extent the fact we neglected the dispersion coupling. We can now write the (relatively) simple expression for the coupling:

$$g \approx 2\frac{N^2}{\Delta^2}\overline{\left(k_2 l\sqrt{\beta_x\beta_y}\right)^2}\,\overline{\delta y^2}$$

In our present case, we may identify $\sqrt{\overline{\delta y^2}}$ as the rms closed orbit deviation; the effect of displacing a sextupole is the same as displacing the beam an equivalent amount in the opposite direction. For our present case, each TME cell contains two pairs of sextupoles, with parameters shown in Table 3. We also need the values μ_x=0.6213, μ_y=0.2271, and $\overline{\gamma\varepsilon_x}$ =3.32 mm mrad, to find that

$$\gamma\varepsilon_y = 14.1\overline{\delta y^2} \qquad (1)$$

Given that we constructed a rather crude model (neglecting for example dispersion coupling which is often significant), there is a good agreement between the coefficient in (1), and the fit obtained from the data shown in Figure 15. This provides some grounds for confidence in the validity of our results.

Table 3

Sextupole parameters. Note that the mean beta functions through the sextupole are given.

	SX	SY
$k_2 l$	59.4 m^{-2}	-47.3 m^{-2}
β_x	2.09 m	0.853 m
β_y	3.41 m	8.289 m

We can also test the model against direct sextupole misalignments, without significant closed orbit deviation, by leaving the quadrupoles properly aligned. The dependence of vertical emittance against rms sextupole vertical misalignment is shown in Figure 16.

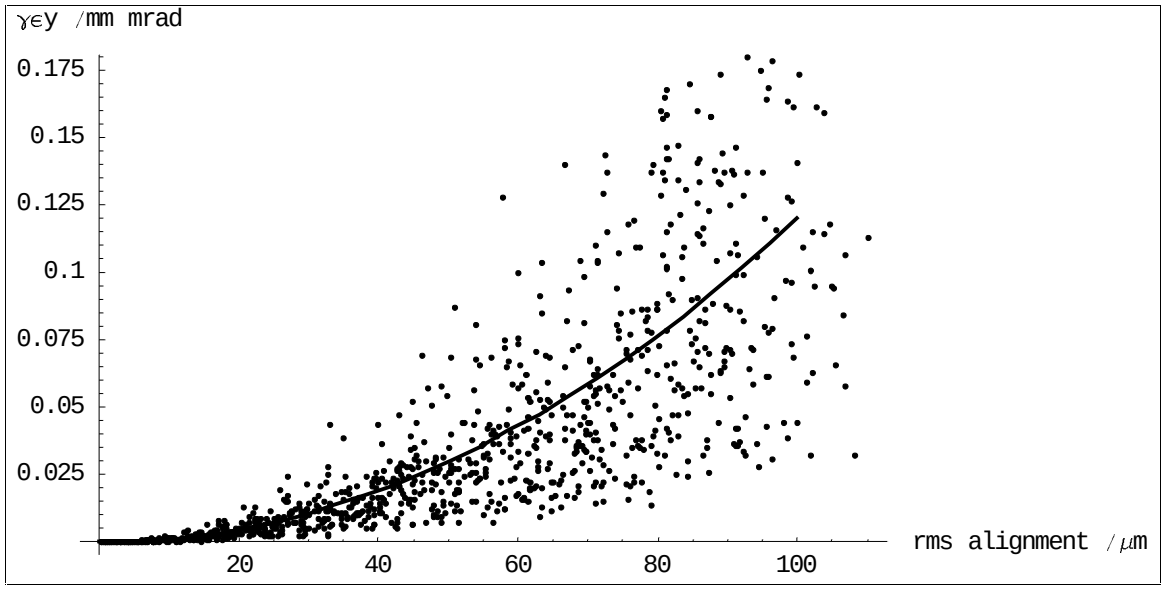

Figure 16

Equilibrium vertical emittance against rms sextupole vertical misalignment, without significant closed orbit deviation (1000 seeds). The line shows a best fit curve, of the form $\gamma\varepsilon_y = 12.0\overline{y^2}$

In this case, the horizontal equilibrium emittance takes the smaller value of 2.67 mm mrad, which is close to the natural emittance of the flat lattice, and our model predicts a value of 11.3 for the coefficient in the quadratic relationship between vertical emittance and rms sextupole misalignment. Again, there is good agreement between the model and the simulation.

We are now in a position to give an initial estimate of the alignment tolerances on the sextupoles. We assume that the closed orbit (as measured through the quadrupoles) may be corrected to the order of a few microns, so that sextupole misalignments are the

dominant contribution to the vertical emittance. The extracted emittance is given in terms of the injected and equilibrium emittances and the store time by:

$$\gamma\varepsilon_{y,ext} = \gamma\varepsilon_{y,inj}\,\mathrm{e}^{-2N_\tau} + \gamma\varepsilon_y\left(1-\mathrm{e}^{-2N_\tau}\right)$$

We assume the injected emittance $\gamma\varepsilon_{y,inj}$ =150 mm mrad, and for the present lattice, the store time is 4.76 (see Table 2). To achieve an extracted emittance of 0.03 mm mrad, therefore we need an equilibrium emittance of 0.0190 mm mrad (0.7% coupling). Using the fitted curve in Figure 16, we therefore expect the rms vertical alignment of the sextupoles to be of the order of 40 μm. Of course, there is significant scatter on the data points, and we need some confidence that the lattice will achieve the required coupling.

Figure 17 shows the distribution of equilibrium vertical emittance with 30 μm rms vertical alignment error on the sextupoles (gaussian distribution, with no cut-off). 92% of cases give an equilibrium vertical emittance below the required value of 0.019 mm mrad. The effects of relaxing the alignment tolerance to 35 μm are shown in Figure 18. The number of cases falling below the equilibrium limit is now only 80%. It should be borne in mind that the closed orbit deviation in both these simulations is effectively zero. More confident values can be placed on the sextupole alignment tolerances once an orbit correction scheme has been designed and incorporated into the simulations. Furthermore, our simulations do not include collective effects, such as intra-beam scattering, that may significantly increase the vertical emittance. It should also be possible to loosen the alignment tolerances on the sextupoles by using skew quadrupoles for local vertical dispersion coupling. In the ZDR, the average vertical emittance was reduced from 2.92×10^{-8} m-rad to 1.43×10^{-8} m-rad using just two skew sextupoles, with a vertical alignment tolerance of 50 μm on the sextupoles[9].

In order to increase the luminosity, it is possible that a lower extracted vertical emittance may be required. For example, an equilibrium vertical emittance of 0.0090 mm mrad (0.34% coupling) will be required to achieve an extracted emittance of 0.02 mm mrad. With a sextupole alignment tolerance of 30 μm, only 51% of cases in our simulation would fall within this limit. To achieve the extracted emittance of 0.02 mm mrad with 90% confidence, an alignment tolerance of 20 μm on the sextupoles is required. The results for this case are shown in Figure 19.

The luminosity is less sensitive to variations in the horizontal emittance, and the horizontal emittance is in turn less sensitive to coupling through vertical closed orbit deviations or sextupole vertical misalignments. However, the horizontal emittance may be significantly affected by horizontal closed orbit deviations arising from quadrupole alignment errors. Without an orbit correction scheme in place, it is not clear what may be achieved in terms of the horizontal closed orbit, though we may look at an illustrative case.

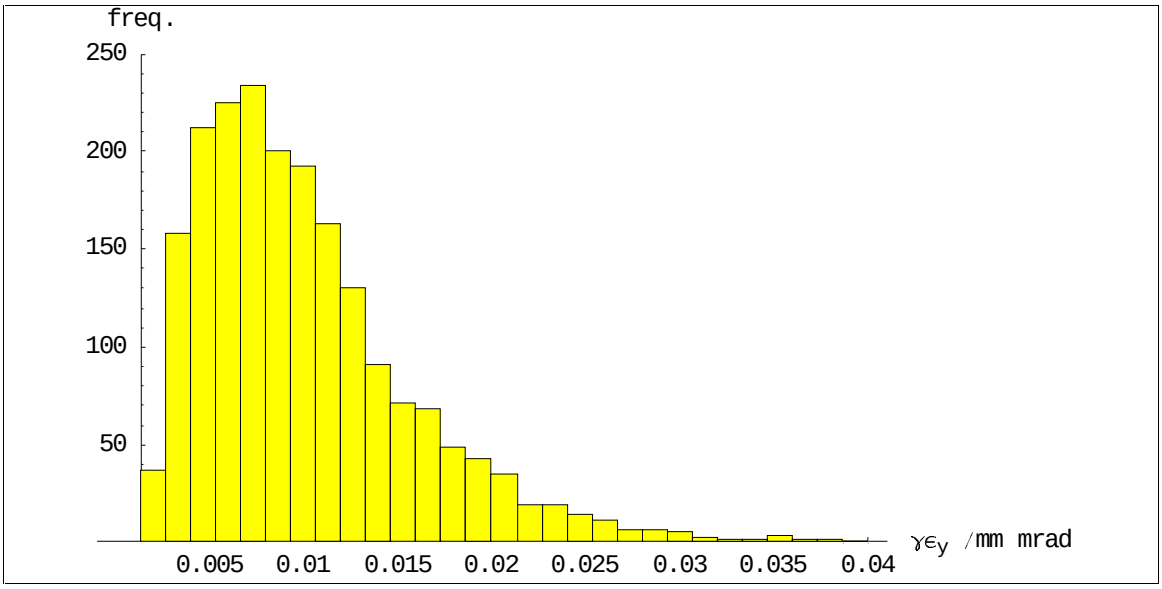

Figure 17

Vertical emittance distribution for 2000 seeds with 30 μm rms vertical alignment error on sextupoles, and zero closed orbit deviation. 92% of cases give $\gamma\varepsilon_y$ < 0.019 mm mrad.

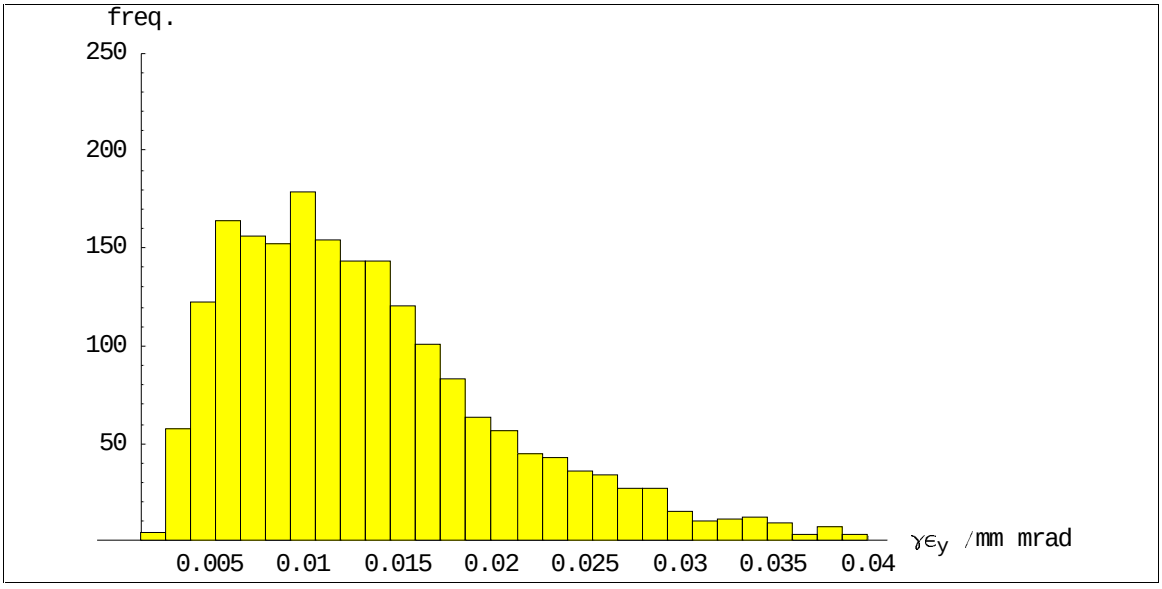

Figure 18

Vertical emittance distribution for 2000 seeds with 35 μm rms vertical alignment error on sextupoles, and zero closed orbit deviation. 80% of cases give $\gamma\varepsilon_y$ < 0.019 mm mrad.

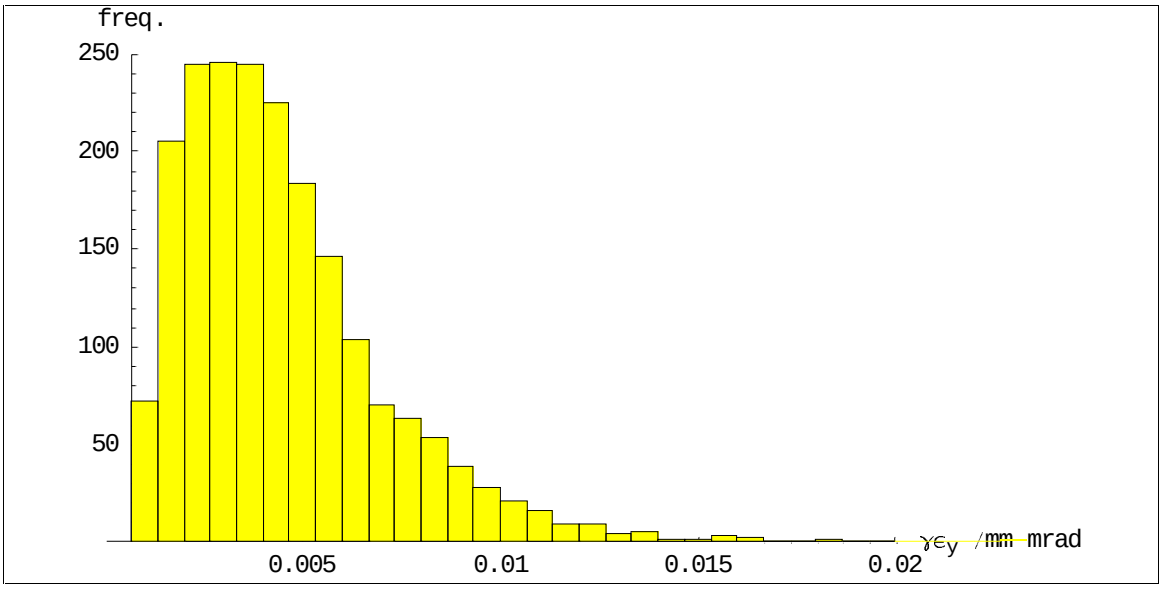

Figure 19

Vertical emittance distribution for 2000 seeds with 20 μm rms vertical alignment error on sextupoles, and zero closed orbit deviation. 94% of cases give $\gamma\varepsilon_y$ < 0.009 mm mrad.

Data were generated by applying a 1 μm rms horizontal alignment error to the quadrupoles. We do not suggest that this alignment tolerance will need to be applied in practice, but in the absence of any orbit correction system in our simulations, this was the level of misalignment needed to give the desired range of closed orbit deviations. There is a strong correlation between equilibrium horizontal emittance and horizontal closed orbit deviation, as shown in Figure 20.

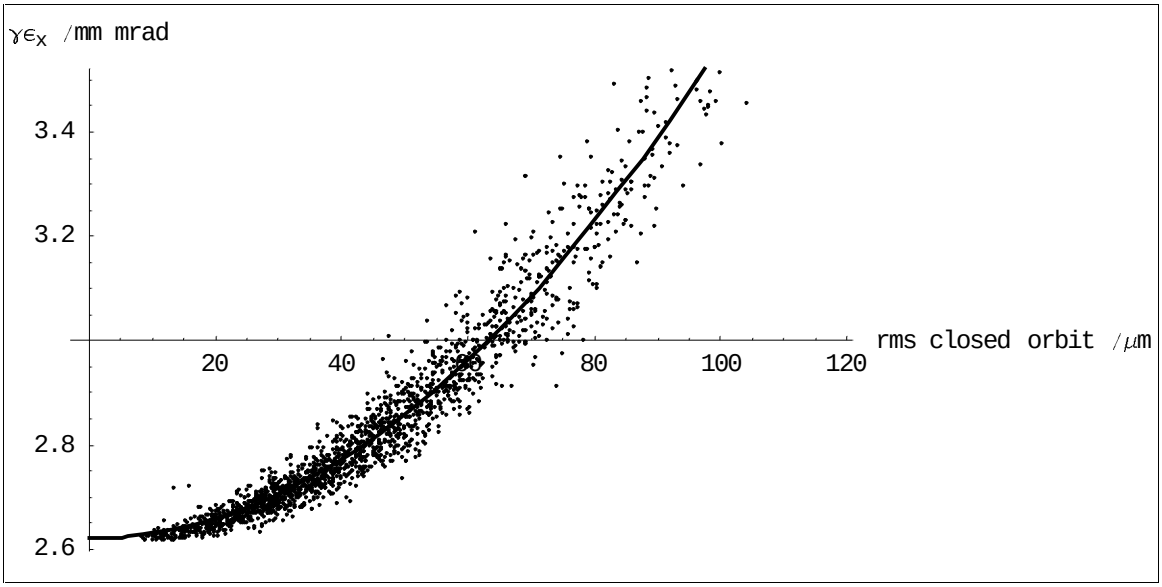

Figure 20

Equilibrium horizontal emittance dependence on horizontal closed orbit (2000 seeds). The line shows a best fit quadratic curve, of the form $\gamma\varepsilon_x = 2.62 + 9.50\times10^{-5}\,\overline{x^2}$

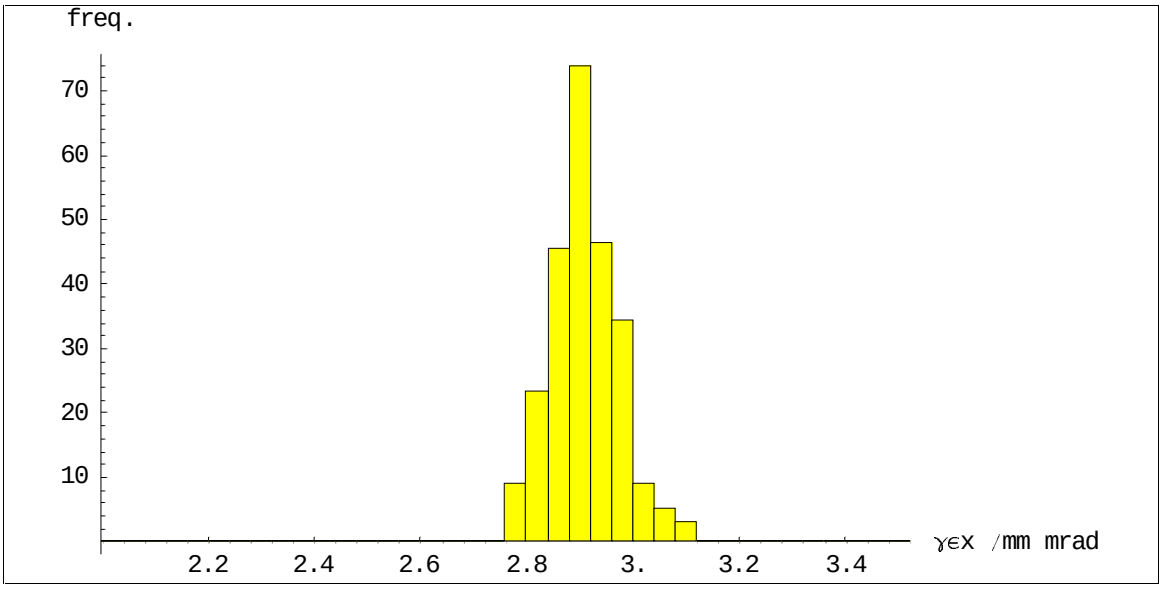

Figure 21

Horizontal emittance distribution with horizontal closed orbit deviation between 50 μm and 60μm rms (247 seeds). 90% of cases give an equilibrium emittance below 2.99 mm mrad.

To achieve the required extracted emittance of 3.0 mm mrad, an equilibrium emittance of 2.99 mm mrad is required. From the data set produced for Figure 20, we selected the 247 cases where the rms closed orbit deviation lay between 50 μm and 60 μm; this subset is shown in Figure 21. 90% of these cases give an equilibrium horizontal emittance below 2.99 mm mrad. Of course, allowing an increase in the horizontal equilibrium emittance will give a direct increase in the vertical emittance, through coupling. Nonetheless, it appears that the horizontal closed orbit correction should be significantly more relaxed than the vertical alignment tolerances.

7 Summary of Magnet Parameters

A summary of the parameters for the magnets used in the present lattice design is shown in Table 4.

Table 4

Magnet parameters in present main damping ring lattice design.

Type	Name	Location	Length	Pole-tip Radius /m	Normalised Field	Pole-tip Field /T	Count
Gradient Sector Dipole	BB	Arc	0.96		$k_0 = 0.1828$ m^{-1} $k_1 = -1.000$ m^{-2}	$B_0 = 1.2$	34
Gradient Sector Dipole	HBBMF	Arc to injection matching	0.48		$k_0 = 0.1828$ m^{-1} $k_1 = -0.5263$ m^{-2}	$B_0 = 1.2$	2
Gradient Sector Dipole	HBBMW	Arc to wiggler matching	0.48		$k_0 = 0.1828$ m^{-1} $k_1 = -0.1860$ m^{-2}	$B_0 = 1.2$	2
Quadrupole	QAF	Arc	0.35	0.02	$k_1 = 5.633$ m^{-2}	0.7436	68
Quadrupole	QAD	Arc	0.25	0.02	$k_1 = -5.912$ m^{-2}	-0.7804	30
Quadrupole	Q2MAF	Arc to injection matching	0.25	0.02	$k_1 = -3.433$ m^{-2}	-0.4532	2
Quadrupole	Q1MAF	Arc to injection matching	0.375	0.02	$k_1 = 5.834$ m^{-2}	0.7701	2
Quadrupole	Q1MF	Arc to injection matching	0.25	0.02	$k_1 = -2.942$ m^{-2}	-0.3883	2
Quadrupole	Q2MF	Arc to injection matching	0.25	0.02	$k_1 = 3.616$ m^{-2}	0.4773	2
Quadrupole	Q1F	Injection straight	0.15	0.02	$k_1 = -1.635$ m^{-2}	-0.2158	2
Quadrupole	Q2F	Injection straight	0.15	0.02	$k_1 = 2.523$ m^{-2}	0.3330	2
Quadrupole	Q3F	Injection straight	0.15	0.02	$k_1 = -1.513$ m^{-2}	-0.1997	2
Quadrupole	Q4F	Injection straight	0.15	0.02	$k_1 = 1.696$ m^{-2}	0.2239	1
Quadrupole	Q2MAW	Arc to wiggler matching	0.25	0.02	$k_1 = -3.223$ m^{-2}	-0.4254	2
Quadrupole	Q1MAW	Arc to wiggler matching	0.375	0.02	$k_1 = 5.738$ m^{-2}	0.7574	2
Quadrupole	Q1MW	Arc to wiggler matching	0.25	0.02	$k_1 = -4.222$ m^{-2}	-0.5573	2
Quadrupole	Q2MW	Arc to wiggler matching	0.25	0.02	$k_1 = 5.001$ m^{-2}	0.6601	2
Quadrupole	Q1W	Wiggler straight	0.15	0.02	$k_1 = -0.1483$ m^{-2}	-0.01958	2
Quadrupole	Q2W	Wiggler straight	0.15	0.02	$k_1 = 2.044$ m^{-2}	0.2698	2
Quadrupole	Q3W	Wiggler straight	0.15	0.02	$k_1 = -1.960$ m^{-2}	-0.2587	1
Sextupole	SX	Arc	0.13	0.02	$k_2 = 456.0$ m^{-3}	0.6019	68
Sextupole	SY	Arc	0.13	0.02	$k_2 = -365.8$ m^{-3}	-0.4829	68

8 Conclusions and Future Direction

The lattice we have described in this note shows significantly better dynamic stability than the previous version of the NLC 180 Hz Main Damping Ring lattice. In particular, the dynamic aperture meets the target of 15 times the injected beam size, although this applies only for the case of on-momentum particles in the flat (correctly aligned) lattice, with the damping wiggler modeled as a linear element.

Initial estimates of sextupole alignment tolerances suggest that 30 μm vertical rms alignment will be required to achieve an extracted emittance below 0.03 mm mrad. This estimate does not take account of closed orbit deviation or collective effects.

The following areas need to be addressed:

- a nonlinear model for the wiggler should be developed, to allow a more realistic determination of the dynamic aperture (this work is in progress);
- an orbit correction system should be drawn up and implemented in the model, to allow more comprehensive studies of the alignment tolerances to be carried out.

9 References

[1] A. Wolski, *"Damping Ring Design for NLC at 180 Hz Repetition Rate"*, CBP Tech Note 216, LCC-0048, October 2000.

[2] H. Nishimura, private communication.

[3] P.Emma and T.O.Raubenheimer, *"Circumference Correction Chicanes for Damping Rings"*, Proceedings PAC 1999.

[4] P.Emma, *"Preliminary Main Damping Ring Design for the NLC (version 2.0)"*, SLAC Memorandum April 23, 1999.

[5] P.Emma and T.O.Raubenheimer, *"Main Damping Ring Design for the NLC"*, Presentation.

[6] MERLIN has been developed by Nick Walker of DESY; we are indebted to him for making this code available to us and supporting its use.

[7] A.W.Chao, *"Evaluation of Beam Distribution Parameters in an Electron Storage Ring"*, J.Appl.Phys. 50(2), February 1979.

[8] H. Nishimura, private communication.

[9] *"Zeroth-Order Design Report for the Next Linear Collider"*, May 1996, pages 155-159.